Trajectory Tracking of a Redundant Hybrid Manipulator Using a Switching Control Method

Atilla Bayram

Abstract—This paper presents the trajectory tracking control of a spatial redundant hybrid manipulator. This manipulator consists of two parallel manipulators which are a variable geometry truss (VGT) module. In fact, each VGT module with 3-degrees of freedom (DOF) is a planar parallel manipulator and their operational planes of these VGT modules are arranged to be orthogonal to each other. Also, the manipulator contains a twist motion part attached to the top of the second VGT module to supply the missing orientation of the end-effector. These three modules constitute totally 7-DOF hybrid (parallel-parallel) redundant spatial manipulator. The forward kinematics equations of this manipulator are obtained, then, according to these equations, the inverse kinematics is solved based on an optimization with the joint limit avoidance. The dynamic equations are formed by using virtual work method. In order to test the performance of the redundant manipulator and the controllers presented, two different desired trajectories are followed by using the computed force control method and a switching control method. The switching control method is combined with the computed force control method and genetic algorithm. In the switching control method, the genetic algorithm is only used for fine tuning in the compensation of the trajectory tracking errors.

Keywords—Computed force control method, genetic algorithm, hybrid manipulator, inverse kinematics of redundant manipulators, variable geometry truss.

I. INTRODUCTION

PARALLEL manipulators are formed by connecting a moving platform to the fixed base via two or more serial kinematics chains. Stewart platform [1], VGT [2] and Delta manipulator [3] can be given as a few examples for this type of manipulators. Compared to their serial counterparts, they have higher precision, rigidity, speed and more payload capacity. On the other hand, these manipulators posses smaller workspace and their controls are very difficult due to their complex kinematics. To alleviate somewhat these deficiencies, some topological multi-loop manipulators are configured by attaching parallel/parallel or parallel/serial manipulators on top of each other. These structures are known as hybrid manipulators widely studied in literature [4]-[6]. Hybrid manipulators have both advantageous and disadvantageous aspects of parallel manipulators.

Redundant manipulators with better mobility have more degrees of freedom than the required ones to fulfill a certain given task. For example, the human robot arm with 7-DOF is a redundant serial manipulator [7]. As well as the main tasks, redundant manipulators can perform some user-defined additional duties such as joint limit avoidance [8], obstacle

Atilla Bayram is with Yuzuncu Yil University, 65080 Van, Turkey (phone: +905373372942; e-mail: atillabayram@yyu.edu.tr).

avoidance [9], singularity avoidance [10], compensation of the fault tolerance in working mode [11] and different type of optimizations [12]. Solving the inverse kinematics solution of these manipulators is pretty hard owing to the fact that the kinematics equations are highly non-linear, the number of solution is infinite and the closed form solution is impossible. Three approaches have been proposed in literature for this solution. The first one is local classical method including the inverse of certain matrices such as Pseudo-inverse, Jacobian transpose represented by Jacobian matrices based on the manipulator geometry. This method presents a solution at the level of velocity and acceleration [13]. Another approximation is global optimization methods which can provide solutions at both position and velocity level. In [14], a method for inverse kinematics of redundant manipulators is suggested at position level with a criterion of having the distance to the obstacles to be maximum while another study in [15] proposed a solution based on an optimization of a penalty function involving the joint limitations. Apart from these methods, the more update solution strategies such as neural network [16], genetic algorithm [17] providing iteratively and globally solutions are used in the kinematics analysis of redundant manipulators.

One of the best ways to test the performance of a manipulator is to follow a given trajectory with the special features assigned. In literature, there are many trajectory tracking control methods, some of which are model based, the others are adaptive. The best examples for the model based controllers frequently used in industries are the calculated torque control (CTC) method [18]-[20]. In this method, the inverse dynamic solution yields the feed forward inputs while the classical PD control is used for feedback parts for errors. Another model based approach is direct dynamic method [21]. Although this method diminishes the computational loads, it is not sensitive in particular to any mass change in systems and gives very slow response according to CTC. In addition to these conventional methods, more current control strategies such as neural network [22], [23], fuzzy [24] and learning iterative [25] methods have also been suggested. They are generally known as adaptive methods which supply the control of manipulator by approximating the estimated values of unknown parameters such as masses, inertias, dimensions, frictions, external disturbances in dynamical model to their real values. However, using this type of controller especially in real-time and fast systems is limited since they bring too much computational burden. Besides, the estimated values cannot be closer to the real ones.

In this study, the trajectory tracking control of a spatial redundant manipulator is presented. The manipulator involves

two parallel modules which are a VGT module with 3-DOF and a rotational actuator connecting the end-effector of the manipulator to the VGT modules for a twist motion. These VGT modules are added on top of each other and their operational planes are orthogonal to each other. As a result, these three modules constitute a hybrid (parallel-parallel) redundant spatial manipulator with 7-DOF. The manipulator is intended to be used in medical operations such as bone drilling, skin cutting etc. Forming the forward kinematics equations, an algorithm is proposed to solve the inverse kinematics. The algorithm contains the solution of the inverse kinematics via an optimization method based on the joint limit avoidance while the manipulator performs the other specified tasks as well. By virtual work principle, the dynamic equations are obtained by using the forward kinematic equations. In order to test the performance of the manipulator and controllers presented, two given trajectories to be tracked precisely are provided as reference curves. The calculated force control (CFC) method is used in these tracking processes. The values of the classical PD (proportional + derivative) gains used in the CFC are adjusted by a switching operation so as to reduce the errors. The gains are normally fixed diagonal matrices determined by trial and error while all matrix elements of the PD gains in this switching mode are set to the variable values by genetic algorithm when a specified error between the desired and real positions is overshoot. This is a hybrid control method switching between the fixed and variable PD gains. Actually, GA provides merely a fine tuning for compensating the trajectory tracking errors.

II. MODELING OF THE MANIPULATOR

The redundant hybrid manipulator is modeled as shown in Fig. 1 with CAD drawing. The manipulator consists of two VGT structures attached on the top of each other and the twist motion part. In fact, each VGT module is a 3-DOF planer parallel manipulator. Because of this, the operational plane of each module is parallel to the motion plane of the VGT module actuators. The operational planes of two successive VGT modules are arranged to be orthogonal to each other. From Fig. 1, the first and second VGT modules move in the $\mathbf{u}_2^{(0)}$ - $\mathbf{u}_3^{(0)}$ and $\mathbf{u}_1^{(1)}$ - $\mathbf{u}_3^{(1)}$ planes and rotate about $\mathbf{u}_1^{(0)}$ and $\mathbf{u}_2^{(1)}$ axes of the respective reference frames attached to these modules. Thus, these two modules form together 6-DOF spatial hybrid manipulator. The twist motion part is a rotational actuator connecting the end-effector of the manipulator to the VGT modules and adds one extra degree of freedom. This part is mounted to the manipulator to compensate the missing rotation about the approach vector ($\mathbf{u}_3^{(p)}$ axis) because this 6-DOF part of the spatial hybrid manipulator cannot provide any rotation about this axis. Considering the whole manipulator with two VGT modules and the twist motion part, it happens to be a 7-DOF spatial hybrid manipulator. In fact, the manipulator is seen like a 6-DOF normal manipulator. However, as seen from Fig. 1, the heave of the top of the manipulator in $\mathbf{u}_3^{(0)}$ direction can be

adjusted via both the first and second VGT modules. Thus, the manipulator itself is a redundant manipulator.

The structure of VGT based modules is set up to be in the shape of a trapezoid rather than a parallelogram. In the VGT modules, the two identical non-diagonal actuators are symmetrically placed according to the motion planes such as the $\mathbf{u}_2^{(0)}$ - $\mathbf{u}_3^{(0)}$ and $\mathbf{u}_1^{(1)}$ - $\mathbf{u}_3^{(1)}$ planes. These structural features enhance the lateral robustness of the manipulator so that it can resist shearing forces and moments more effectively.
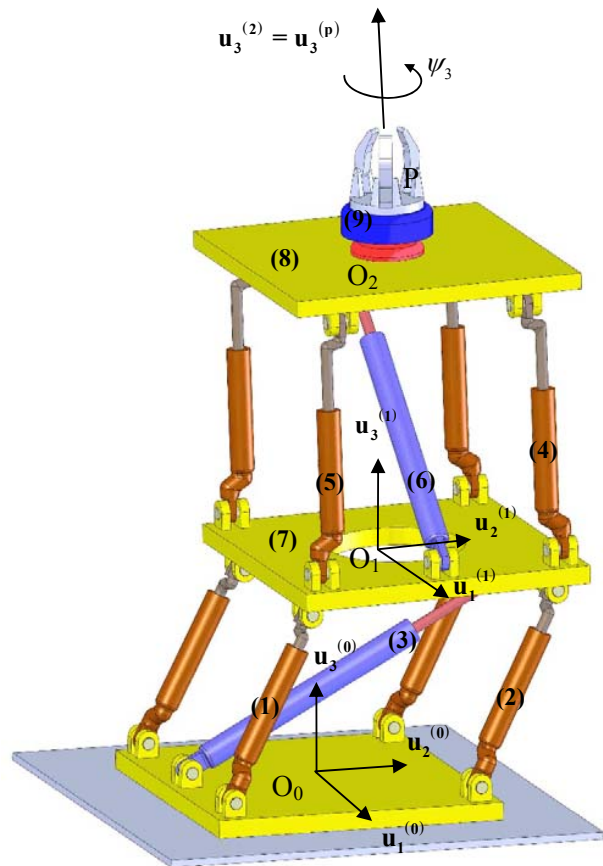

Fig. 1 Hybrid spatial redundant manipulator with 7-DOF

III. FORWARD KINEMATICS ANALYSIS

The forward kinematics yields a solution for the tip point position of the manipulator and the orientation of the end-effector in terms of the independent joint variables. This analysis involves also the calculations of passive joint variables in the VGT modules. Referring to Fig. 2, the passive joint variables and the position vector belonging to the first and second VGT modules can be calculated based on the dimensions and independent joint variables.

The loop closure equations for the first VGT module can be obtained according to the loops of $A_0B_0B_{11}$ and $A_0B_{11}A_{11}$. The equations are written in terms of s_1, v_1, p_1, s_2, v_2, p_2 and ψ_3 which are the independent joint variables and dimensions of b and d as:

$$2b + v_1 \cos(\gamma_1) = p_1 \cos(\beta_1) \tag{1}$$

$$v_1 \sin(\gamma_1) = p_1 \sin(\beta_1) \tag{2}$$

$$s_1 \cos(\alpha_1) + 2d \cos(\theta_1) = p_1 \cos(\beta_1) \tag{3}$$

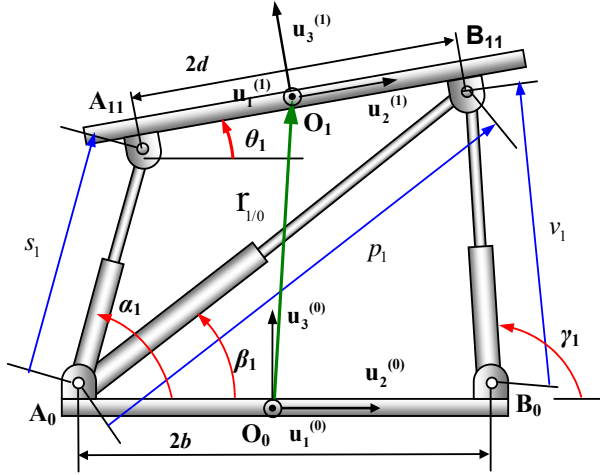$$s_1 \sin(\alpha_1) + 2d \sin(\theta_1) = p_1 \sin(\beta_1) \tag{4}$$

Fig. 2 The planar representation of the first VGT module

For the equations of the second VGT module, the procedure is only to replace the following notation and the motion plane.

$$\alpha_1 \to \alpha_2, \ \beta_1 \to \beta_2, \ \gamma_1 \to \gamma_2, \ \theta_1 \to \theta_2, \ s_1 \to s_2, \ v_1 \to v_2,$$
$$p_1 \to p_2.$$

The calculations of the passive joint variables in terms of the independent joint variables can be found in detail in [26]. According to Fig. 1, the tip point position vector of the manipulator can be written as:

$$\mathbf{r_p} = \mathbf{r_{0P}} = \mathbf{r_{01}} + \mathbf{r_{12}} + \mathbf{r_{2P}} \tag{5}$$

where $\mathbf{r_{01}}$, $\mathbf{r_{12}}$ and $\mathbf{r_{2p}}$ are the position vectors connecting the related centers of the coordinate axes (O_0, O_1, O_2 and P). These vectors can be expressed in matrix form relative to base reference frame as:

$$\mathbf{r_{P/0}^{(0)}} = \mathbf{r_{1/0}^{(0)}} + \hat{\mathbf{C}}^{(0,1)} \mathbf{r_{2/1}^{(1)}} + h_1 \hat{\mathbf{C}}^{(0,2)} \mathbf{u_3^{(2)}} \tag{6}$$

In this expression, h_1 stems from the height of the rotational actuator carrying the end-effector and $\hat{\mathbf{C}}^{(i,j)}$ is an orientation matrix of each coordinate frame.

$$\hat{\mathbf{C}}^{(0,1)} = e^{\tilde{u}_1 \theta_1} \tag{7}$$

$$\hat{\mathbf{C}}^{(0,2)} = e^{\tilde{u}_1 \theta_1} e^{\tilde{u}_2 \theta_2} \tag{8}$$

$\mathbf{r_{1/0}^{(0)}}$ and $\mathbf{r_{2/1}^{(1)}}$ position vectors can be expressed in matrix form relative to the base and second frames attached to the top of the first and second VGT modules respectively as:

$$\mathbf{r_{1/0}^{(0)}} = \left(s_1 \cos\alpha_1 + d_1 \cos\theta_1 - b_1 \right) \mathbf{u_2} + \left(s_1 \sin\alpha_1 + d_1 \sin\theta_1 \right) \mathbf{u_3} \tag{9}$$

$$\mathbf{r_{2/1}^{(1)}} = \left(-s_2 \cos\alpha_2 - d_1 \cos\theta_2 + b_1 \right) \mathbf{u_1} + \left(s_2 \sin\alpha_2 + d_1 \sin\theta_2 \right) \mathbf{u_3} \tag{10}$$

The orientation of the end-effector can be calculated in matrix form as:

$$\hat{\mathbf{C}}^{(0,3)} = \hat{\mathbf{C}}^{(0,1)} \hat{\mathbf{C}}^{(1,2)} \hat{\mathbf{C}}^{(2,3)} = e^{\tilde{u}_1 \theta_1} e^{\tilde{u}_2 \theta_2} e^{\tilde{u}_3 \psi_3} \tag{11}$$

The knowledge about the exponential notation of rotation matrices can be found in reference [27].

IV. THE INVERSE KINEMATICS OF THE MANIPULATOR

Redundant manipulators do not have not only inherently redundancy but also the tasks existed can make any manipulator redundant. For example, 6-DOF spatial manipulator becomes redundant for a path following in 3D space with free orientation. In this study, the hybrid manipulator is inherently redundant and its redundancy is increased when it is used for trajectory tracking with free orientation in a spatial task. To solve the general inverse kinematics of the manipulator, we constituted 14 equations, which are the top point position vector (6), orientation matrix of the end-effector (11) and the loop closure equations (1)-(4) obtained in the forward kinematics analysis, versus 15 unknowns, which are 7 independent joint variables and 8 passive joint variables. The inverse kinematics of this 7-DOF redundant manipulator turns into the redundancy resolution based on optimization of a cost function. The manipulator uses the prismatic joints as the actuators except for the last one, which is rotational actuator. There is a restriction on the joint variables which are the leg lengths of the actuators varying between the maximum and minimum elongation. Thus, the cost function for redundancy resolution is chosen for the joint limit avoidance as.

$$\Phi(\mathbf{q}) = \frac{1}{n} \sum_{i=1}^{n} \left(\frac{q_i - q_i^*}{q_{iM} - q_{im}} \right)^2 \tag{12}$$

where q_{iM} and q_{im} are the maximum and minimum joint lengths, q_i is the real joint value and $q_i^* = (q_{iM} + q_{im})/2$ is the middle value of the joint variation. This optimization tries to ensure that the joint variables be within the range of joint limits when the manipulator performs the specified positional and orientation tasks. The redundancy resolution is solved at position level for the inverse kinematics via "fmincon" command in MATLAB Optimization Toolbox with the equality constraints and the joint limits of $0 < q_{im} \leq q_i \leq q_{iM}$. Taking the first and second time derivatives of the joint

variables found gives us the feasible $\dot{\mathbf{q}}(\mathbf{t})$ and $\ddot{\mathbf{q}}(\mathbf{t})$ rates in joint space. Thus, the desired trajectories in Cartesian space can be mapped into in the joint space with the position, velocity and acceleration terms.

V. TRAJECTORY TRACKING CONTROL

A. Dynamic Analysis

Dynamic analysis is particularly important for a manipulator moving with quite high velocities and accelerations. It is also essential for the model-based control of manipulators. Newton-Euler [28], Lagrange [29] and Virtual Work Principle [30] have been proposed in literature to obtain dynamic equations of manipulators. The redundant hybrid manipulator presented in this paper has some moving reverence frames relative to the base and also many passive joints stemming from the closed loop mechanisms. These reveals a very non-linear complicated and coupled dynamic equation set. In the dynamic analysis, some assumptions are made to reduce the computational burden for the fast responses. For example, the frictions are considered to be merely on the linear actuators and the masses of the actuators used in VGT modules are distributed onto the upper and lower moving platforms.

Based on the Virtual Work Principle and the forward kinematics expressed in Section III, the dynamic equation of the redundant hybrid manipulator is defined as:

$$\sum_{i=1}^{N} \left[\mathbf{J}_{\mathbf{V},i} \left(m_i \left(\mathbf{a}_{ci} - \mathbf{g} \right) - \mathbf{F}_i \right) + \mathbf{J}_{\omega,i} \left(\mathbf{I}_i \dot{\boldsymbol{\omega}}_i + \tilde{\boldsymbol{\omega}}_i \mathbf{I}_i \boldsymbol{\omega}_i - \mathbf{T}_i \right) \right] = 0 \tag{13}$$
$$i = 1, 2, 3$$

Where $\mathbf{J}_v$ and $\mathbf{J}_\omega$ are the translational and rotational Jacobian matrices, respectively and $\mathbf{a}_{ci}$ and $\dot{\boldsymbol{\omega}}_i$ are the linear and angular acceleration of center of gravity of each link relative to the fixed base reference frame. Since these acceleration terms also involve the passive joint variables we need to represent them by the independent joint variables as:

$$\left. \begin{array}{l} \mathbf{a}_{ci} = \mathbf{A}_{\mathbf{V},i} \ddot{\mathbf{q}} + \mathbf{u}_i \\ \dot{\boldsymbol{\omega}}_i = \mathbf{A}_{\omega,i} \ddot{\mathbf{q}} + \mathbf{w}_i \end{array} \right\} \quad i = 1....3 \tag{14}$$

where $\mathbf{A}_\mathbf{V}$ and $\mathbf{A}_\omega$ are the translational and rotational transformation matrices between the acceleration terms and the independent joint variables. With (14), the dynamic equation of motion in terms of the independent joint variables is represented as:

$$\mathbf{M}(\mathbf{q}) \ddot{\mathbf{q}} + \mathbf{C}(\mathbf{q}, \dot{\mathbf{q}}) = \mathbf{F} - \mathbf{J}^{\mathbf{T}} \mathbf{F}_e \tag{15}$$

$\mathbf{M}(\mathbf{q})$ is the inertia matrix, $\mathbf{C}(\mathbf{q}, \dot{\mathbf{q}})$ involves the Coriolis, gravity and viscous damping forces, $\mathbf{J}^{\mathbf{T}} = \begin{bmatrix} \mathbf{J}_v & \mathbf{J}_\omega \end{bmatrix}$ is Jacobian matrix, $\mathbf{F}$ is the actuator forces and $\mathbf{F}_e$ is the disturbance and cutting forces. The cutting force is represented

as a reaction force between the cutting tool of the robot at the end-effector and the material to be processed. The cutting force can also be calculated at the reverse direction to the velocity vector of the tip point of the manipulator as:

$$\mathbf{F}_e = \mathbf{J}_\mathbf{V} \left[\frac{-\mathbf{V}}{|\mathbf{V}|} \mathbf{F}_0 + \mathrm{rand} \left(\mathbf{F}_\mathbf{d} \right) \right] \tag{16}$$

$$\mathbf{V} = \mathbf{J}_\mathbf{V} \, \dot{\mathbf{q}} \tag{17}$$

In the calculations, F_0 is taken as a fixed predicted value for the cutting force and $\mathbf{F}_\mathbf{d}$ is a disturbance force.

Due to the principle of virtual work, the constraint forces and interacting forces are eliminated to formulate the inverse dynamics of the manipulator. Equation (15) governing the system motion is used to develop control laws.

B. Computed Force Control (CFC) Method

This method is called "computed torque control" in literature due to rotary actuators generally used in robot manipulators. We use the name of "computed force control" since the actuators are prismatic. Computed torque method is known as a special application of the feedback linearization of the nonlinear system and is a model based method. The kinematics and dynamic equations studied in the previous sections of this paper are used to evaluate the control of the manipulator via the computed force control method. The CFC uses the linearized and decoupled manipulator dynamics with the classical PD feedback loop as shown in the following equations.

Write the computed force for the manipulator,

$$\mathbf{F} = \mathbf{M}(\mathbf{q}) \ddot{\mathbf{q}}_{\mathrm{ref}} + \mathbf{C}(\dot{\mathbf{q}}, \mathbf{q}) \tag{18}$$

where $\ddot{\mathbf{q}}_{\mathrm{ref}}$ is a control input defined as

$$\ddot{\mathbf{q}}_{\mathrm{ref}} = \ddot{\mathbf{q}}_\mathbf{d} + \mathbf{K}_\mathbf{p} \mathbf{e} + \mathbf{K}_\mathbf{v} \dot{\mathbf{e}} \tag{19}$$

$\mathbf{e} = \mathbf{q}_\mathbf{d} - \mathbf{q}$ is position error, $\mathbf{q}_\mathbf{d}$, $\dot{\mathbf{q}}_\mathbf{d}$ and $\ddot{\mathbf{q}}_\mathbf{d}$ are the desired position, velocity and acceleration of the independent joint variables, respectively. $\mathbf{K}_\mathbf{p}$ and $\mathbf{K}_\mathbf{v}$ are the position and velocity feedback gains selected correspondingly to make this error equation stable. Global asymptotic stability of this equation is proved in detail in [18]. The computed forces are calculated as

$$\mathbf{F} = \mathbf{M}(\mathbf{q}) \left[\ddot{\mathbf{q}}_\mathbf{d} + \mathbf{K}_\mathbf{p} \mathbf{e} + \mathbf{K}_\mathbf{v} \dot{\mathbf{e}} \right] + \mathbf{C}(\dot{\mathbf{q}}, \mathbf{q}) \tag{20}$$

From the inverse dynamics, the joint variables can be calculated under the external forces, $\mathbf{F}_e$ and the disturbance forces, $\mathbf{F}_\mathbf{d}$ randomly assigned. The condition on the disturbance is assigned as $\|\mathbf{F}_\mathbf{d}\| < \eta$. As a result, the second joint rates can be calculated by (15) as:

$$\ddot{\mathbf{q}} = \mathbf{M}^{-1}\left[\mathbf{F} - \mathbf{C}(\dot{\mathbf{q}},\mathbf{q}) - \mathbf{J}^{\mathbf{T}}\mathbf{F_e}\right] \qquad (21)$$

The position and velocity of the joints are solved with the Euler numerical integration method by using (21). The following procedure is applied to trace the given trajectory as closely as possible.

- For the desired trajectory vector $\mathbf{r(t)}$, the independent joint variables $\mathbf{q(t)}$ are solved at position level by using the kinematics equations in (1) to (11) and the cost function in (12) over the joint limits, $0 < q_i^{min} \le q_i \le q_i^{max}$.
- The first and second rates of the joint variables are calculated via the Euler integration method with the result of the previous step.
- Select the feedback PD control gains $\mathbf{K_p}$ and $\mathbf{K_v}$ for the computed force control and switching control methods.
- Take $\mathbf{K_p}$ and $\mathbf{K_v}$ as fixed diagonal matrices for all time steps.
- Take $\mathbf{K_p}$ and $\mathbf{K_v}$ as variable gain matrices for each time step by GA for fine tuning.

Finally, all simulations are fulfilled in MATLAB regarding to the desired trajectory and manipulator specifications.

C. Switching Control Method (SCM)

Sometimes, solutions for harder optimization problems cannot be easily carried out by conventional optimization methods. Genetic algorithm can be easily applied to these types of optimization problems. GA is a nondeterministic stochastic search algorithm based on the mechanism of natural selection and natural genetics [31]. Applying the mechanics of GA, the solutions are obtained by mapping the real values into binary codes and processing these codes.

In CFC method, the feedback gain matrices of classical PD control are taken as fixed one in each time step. This is generally a better approach for trajectory tracking of manipulators in real time applications. However, this fixed matrix approximation cannot be sufficient for convenient tracking errors, especially for in curvedly trajectories. Thus, we need to use a fine tuning to compensate the errors which are out of the acceptable limits. For this aim, genetic algorithm is an effective approach to select the feedback gains for a better control of the manipulator. Actually, GA cannot be used alone in real time applications because it requires an excessive computation time and sometimes a premature convergence may occur in calculations. So, we use merely GA together with CFC method to eliminate errors exceeding a certain value. That is, a switching takes place between CFC and GA algorithm in a small number of time steps until the error decreases below a specified acceptable value. Because of this, this method is called "Switching Control Method". In this paper, $\mathbf{K_p}$ and $\mathbf{K_v}$ consist of 7 by 7 matrices, i.e., each has 49 elements, each of which is represented by 8 bit. To calculate $\mathbf{K_p}$ and $\mathbf{K_v}$, the population of the genetic algorithm contains totally 784 bits for each generation. The elements of gain matrices vary between a maximum and minimum values by changing "0" and "1" bits as:

$$K_p^{min} \le \left[K_p\right]_{ij} \le K_p^{max} \text{ and } K_v^{min} \le \left[K_v\right]_{ij} \le K_v^{max}$$
$$i, j = 1, 2, \ldots, 7 \; .$$

Fig. 3 summarizes graphically the procedure of the CFC method and SCM.

When CFC is not enough for errors, GA will be activated to select the best PD gain matrices to decrease the error. The mechanics of GA is depending on choosing of the best population according to the fitness function which is the Euclidian norm of the trajectory errors. In each loop, GA generates many populations. The mechanics of GA selects a set of better populations with smaller fitness values while the others are discarded. At the end of the generation loop, the population with the best fitness is chosen as an elite population for $\mathbf{K_p}$ and $\mathbf{K_v}$ making the errors smaller.

VI. Simulation and Results

In simulations, we focused only on the position of the tip point of the manipulator for the trajectory tracking. In this process, the orientation of the end-effector was kept to be free. Two desired test curves are given as the case studies.

A. Case Study 1

The trajectory defines a closed parametric curve within the workspace for the convenient parameters of $\mathbf{X_0}$, $\mathbf{Y_0}$, $\mathbf{Z_0}$, $\mathbf{a_X}$, $\mathbf{a_Y}$ and $\mathbf{a_Z}$ as shown in Fig. 4.

$$\begin{aligned} \mathbf{X} &= \mathbf{X_0} + \mathbf{a_X}\sin(t) \\ \mathbf{Y} &= \mathbf{Y_0} + \mathbf{a_Y}\cos(t) \\ \mathbf{Z} &= \mathbf{Z_0} + \mathbf{a_Z}\sin(2t)\cos(2t) \end{aligned} \qquad (22)$$
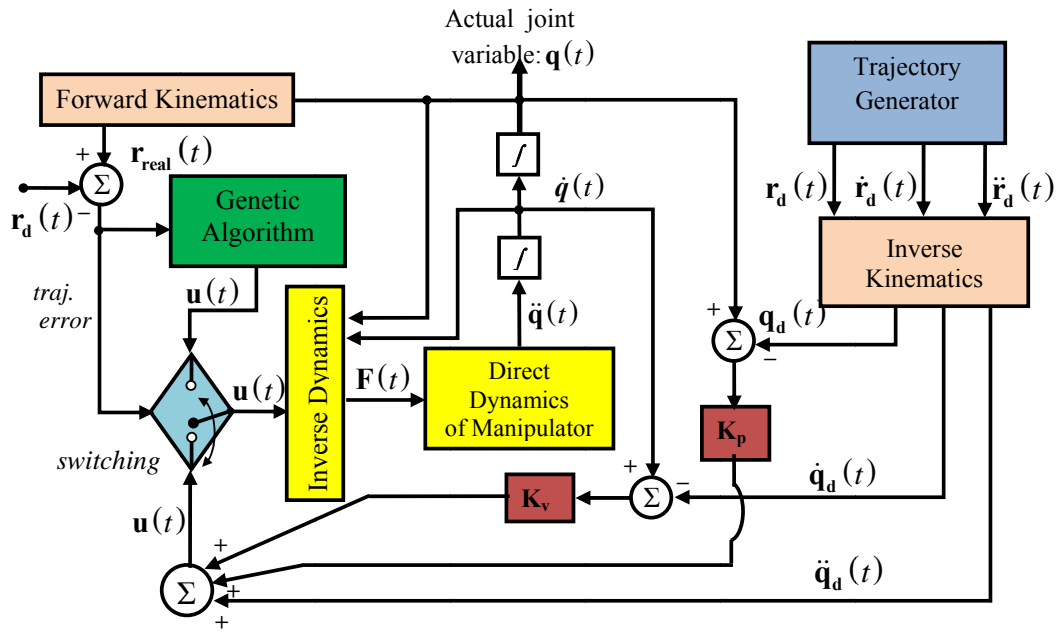
Fig. 3 The graphic representation of the CFC and SCM methods

For this task, the feedback fixed gain matrices for the CFC are selected by trial and error as $\mathbf{K_p} = \text{daig}[5 \ 5 \ 5 \ 5 \ 5 \ 5 \ 5]\times10^3$, $\mathbf{K_v} = \text{daig}[3 \ 3 \ 3 \ 3 \ 3 \ 3 \ 3]\times10^2$. All specifications and manipulator parameters are given in Appendix. In the SCM, the gains are calculated step by step by GA minimizing the trajectory errors. In simulations, each element of the gain matrices varies between a minimum and maximum value such as $\left[\mathbf{K_p}\right]_{ij} = [0-5,000]$ and $\left[\mathbf{K_v}\right]_{ij} = [0-300]$. The compared outcomes of the simulation are shown in Figs. 4-6. Fig. 4 shows the desired and actual trajectories while Fig. 5 shows the absolute errors between the desired and actual positions for fixed and variable $\mathbf{K_p}$ and $\mathbf{K_v}$ matrices. The maximum error for the switching control method is 0.48 mm while it is 0.53 mm for the CFC method. In fact, from Fig. 5, these errors occur in a very short time. However, after very small number of time step, both methods yield very convenient results. The errors remain below 0.2 mm along the entire trajectory. For the SCM, the threshold error value is selected 0.2 mm. If this value is assigned to lower one, the SCM can generate a trajectory with the errors smaller than specified one. Finally, during this task operation, Fig. 6 shows the calculated actuator forces of the VGT modules. In this figure, some peaks and troughs indicate that the SCM is activated in the control of the trajectory tracking. Smaller threshold error values cause highly oscillatory force behavior because the system has coupled PD gain matrices and the calculation of these gains can be performed randomly in different domains without depending on the previous outcomes. In this case study, the external forces are excluded for the sake of the simplicity.
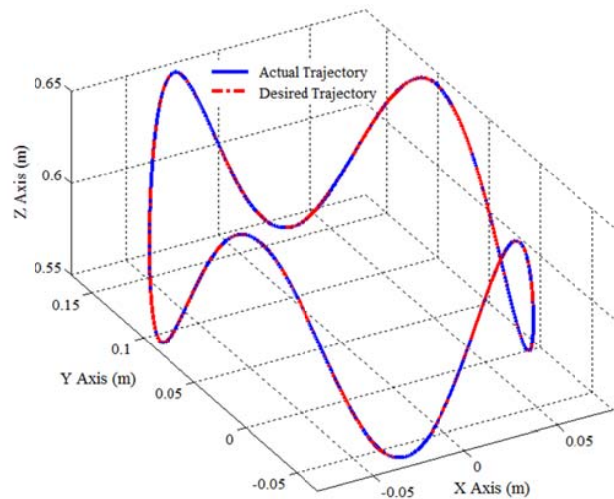

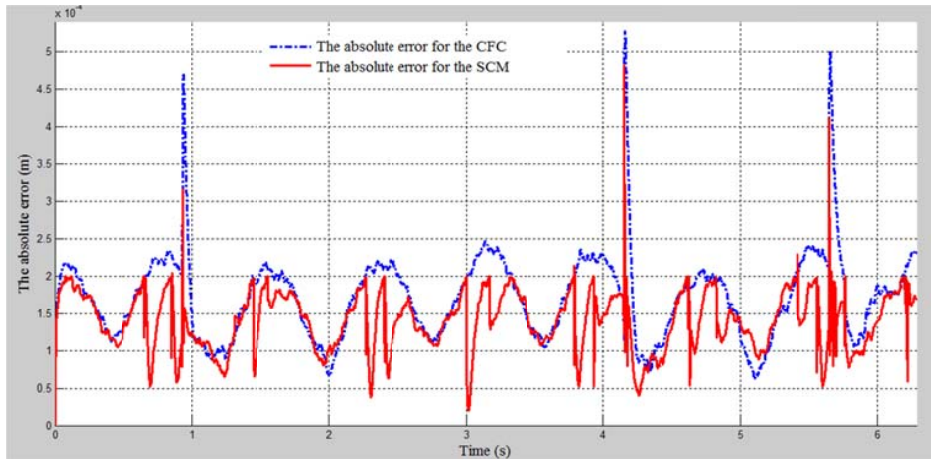Fig. 4 Trajectory tracking of the hybrid redundant manipulator

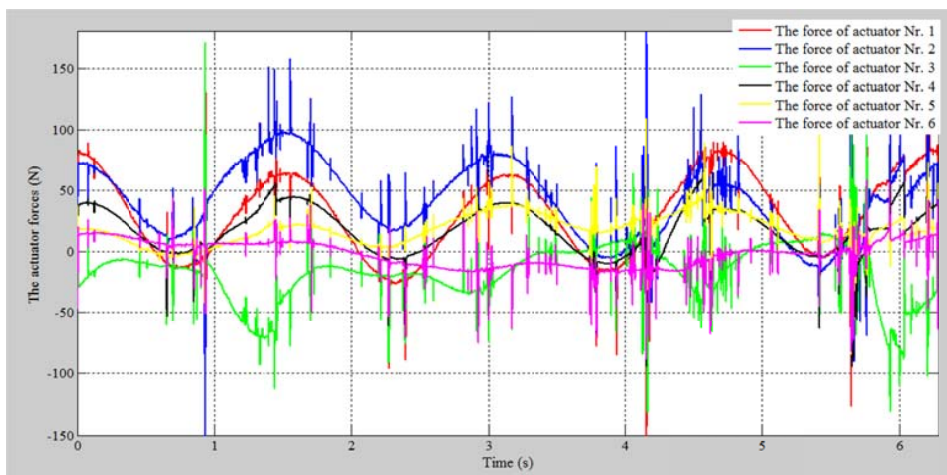Fig. 5 The absolute position error between the actual and desired trajectories

Fig. 6 Linear actuator forces of the hybrid redundant manipulator

B. Case Study 2

The second reference trajectory is given in cubic function as a form.

$$\mathbf{T}(t) = \mathbf{c_3}t^3 + \mathbf{c_2}t^2 + \mathbf{c_1}t + \mathbf{c_0} \qquad (23)$$

This reference trajectory $\mathbf{T}(t)$ defines two piecewise parametric spatial lines within the workspace of the hybrid manipulator as shown in Fig. 7. The first time rates of the lines are zero at corners. The feedback gains are selected as $\mathbf{K_p} = \text{daig}[15 \quad 15 \quad 15 \quad 15 \quad 15 \quad 15 \quad 15] \times 10^3$, and $\mathbf{K_v} = \text{daig}[6 \quad 6 \quad 6 \quad 6 \quad 6 \quad 6 \quad 6] \times 10^2$. The cutting and disturbance forces as an external force are considered in this case study. The results of the simulations are shown in Figs. 7-9. Fig. 7 shows the desired and actual trajectories while Fig. 8 shows the absolute errors between the desired and actual positions with and without the external forces.
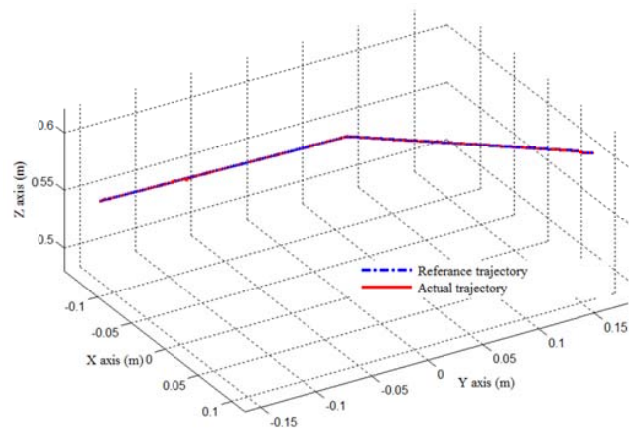

Fig. 7 Trajectory tracking of the hybrid redundant manipulator

As shown in Fig. 8, the external forces affected the trajectory error pretty much. The maximum absolute positional error for this part is 0.68 mm whereas the simulation without external forces provides the maximum

error of 0.31 mm. The interesting results appeared for the SCM with the smaller trajectory errors. This control method can keep the errors in a desired level. For example, it cannot exceed 0.2 mm for without external forces and 0.4 mm for the external forces. However, as seen in Fig. 9, these approach results in quite fluctuated actuator forces.
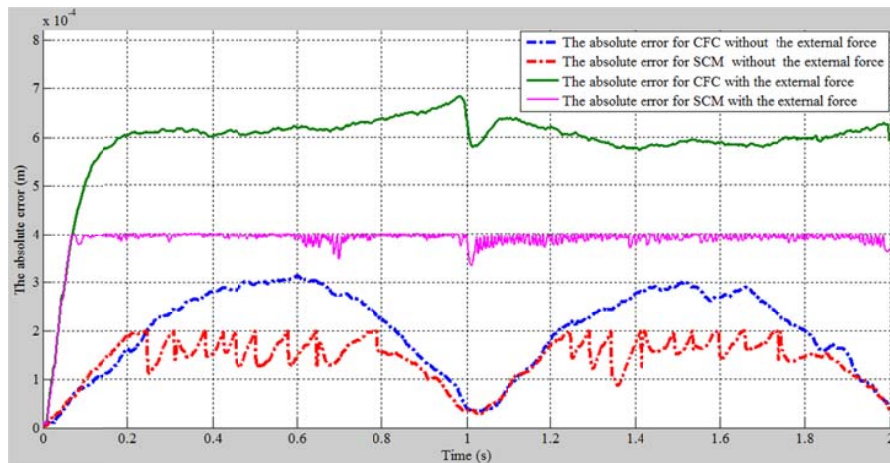

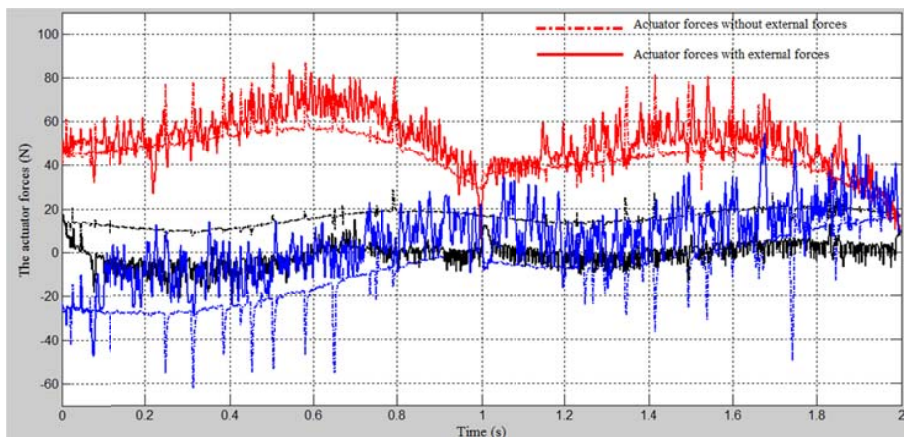Fig. 8 The absolute position error between the actual and desired trajectories

Fig. 9 Linear actuator forces of the hybrid redundant manipulator

VII. DISCUSSION AND CONCLUSIONS

In this paper, we presented a redundant hybrid manipulator with seven degrees of freedom. For the trajectory tracking in 3D space, the inverse kinematics of the manipulator is carried out according to the joint limit avoidance at position level. Although the manipulator possesses the joint constrains and the solutions need cumbersome calculations, the method gives the better results for accuracy and timing. For the desired trajectories, the manipulator could try to follow them by using the inverse kinematic solution, the dynamic equations and the computed force control and switching methods. From the case studies, the simulation outcomes with the proposed methods in this paper are very satisfactory compared to similar studies in literature. Mostly, even if the results are consistent with the literature, it is expected that the positional errors should be held at micrometer level rather than millimeter. To decrease the errors, the feedback gains were increased enormously. This brings about an inconvenience of more excessive actuator forces, i.e., energy consumption, and causes an undesirable vibration on the actuators. For this aim, the genetic algorithm is proposed to make the fine tuning of the PD controller with smaller feedback gains. From the figures and data, the switching control method via GA has superiority on the classical approach and could considerably reduce the errors. However, in addition to the premature convergence, GA has a drawback that all generation loops take longer times and also gives the larger and fluctuated actuator forces. Thus, this can restrict the GA method to use in online implementations. So as to get the advantages of these two methods and to avoid the computational burden for the GA and reach the accurate trajectories, the combined method was proposed by switching between the CFC and GA for compensation of errors. This redundant hybrid manipulator is intended for use in medical operations such as bone drilling, skin cutting. Therefore, for a future work, the control of the manipulator needs further improvement. The excessive actuator forces are still a problem

for both methods. To overcome this problem, non-traditional controllers can be designed or the redundancy resolution of the manipulator can be tackled to minimize the actuator forces.

APPENDIX

A. The Features of the Manipulator

The concentrated masses of platforms (the link numbers of 7, 8 and 9 shown in Fig. 1):

$$m_7 = 2.75 \text{ kg} ;$$
$$m_8 = 2.75 \text{ kg} ;$$
$$m_9 = 0.75 \text{ kg} ,.$$

The inertias:

$$I_7 = \begin{bmatrix} 18.42 & 0 & 0 \\ 0 & 18.47 & 0 \\ 0 & 0 & 36.77 \end{bmatrix} \times 10^{-3} \text{ kg.m}^2$$

$$I_8 = \begin{bmatrix} 17.59 & -0.09 & 0 \\ -0.09 & 17.51 & 0 \\ 0 & 0 & 34.64 \end{bmatrix} \times 10^{-3} \text{ kg.m}^2$$

$$I_9 = \begin{bmatrix} 0.654 & 0 & 0 \\ 0 & 0.654 & 0 \\ 0 & 0 & .884 \end{bmatrix} \times 10^{-3} \text{ kg.m}^2$$

The viscous friction coefficient: $c = 200 \ Ns/m$

The norm of disturbance force: $\eta = \begin{bmatrix} 5 \\ 5 \\ 5 \end{bmatrix} \ (N)$

The predicted nominal external force: $F_0 = 20 \ (\text{N})$

B-The Parameters of the Genetic Algorithm:

- The crossover type: *uniform crossover*
- The probability of crossover: 0.6
- The mutation probability (per bit): 0.001
- The selection type*: The Stochastic Universal Sampling method*
- The size of the population: 50
- The maximum number of generations: 50
- The crossover type: *uniform crossover*
- The selection type*: The Stochastic Universal Sampling method*

REFERENCES

[1] X. S. Gao, D. Lei, Q. Liao and G. F. Zhang, "Generalized Stewart Gough platforms and their direct kinematics," *IEEE Transactions on Robotics*, vol. 21, no. 2, pp 141-151, April 2005.

[2] P. C. Hughes, W. G. Sincarsin and K. A. Carroll, "Trussarm—a variable-geometry-truss manipulator," *Journal of Intelligent Material Systems and Structures*, 1991, 2.2: 148-160, 1991.

[3] A. Codourey, "Dynamic modeling and mass matrix evaluation of the DELTA parallel robot for axes decoupling control," *Intelligent Robots and Systems' 96, IROS 96, Proceedings of the 1996 IEEE/RSJ International Conference* on. Vol. 3. IEEE, 1996.

[4] K. Daniel, P. Wenger and D. Chablat, "Kinematic analysis of a serial–parallel machine tool, The VERNE machine" *Mechanism and Machine Theory*, 44.2 , 487-498, 2009.

[5] F. Gómez-Bravo, G. Carbone and J. C. Fortes, "Collision free trajectory planning for hybrid manipulators," *Mechatronics*, 22.6, 836-851, 2012.

[6] Z. Gao, and Z. Dan, "Performance analysis, mapping, and multiobjective optimization of a hybrid robotic machine tool," *Industrial Electronics, IEEE Transactions* on 62.1, 423-433, 2015.

[7] H. M. Do, C. Park, and J. H. Kyung, "Dual arm robot for packaging and assembling of IT products," *Automation Science and Engineering (CASE), 2012 IEEE International Conference* on. IEEE, p. 1067-1070, 2012.

[8] A. Atawnih, P. Dimitrios, and D. Zoe, "Kinematic control of redundant robots with guaranteed joint limit avoidance," *Robotics and Autonomous Systems,* 2016.

[9] Y. Zhang and W. Jun, "Obstacle avoidance for kinematically redundant manipulators using a dual neural network," *Systems, Man, and Cybernetics, Part B: Cybernetics, IEEE Transactions* on 34.1, 752-759, 2004.

[10] S. Chiaverini, "Singularity-robust task-priority redundancy resolution for real-time kinematic control of robot manipulators," *Robotics and Automation, IEEE Transactions on* 13.3, 398-410, 1997.

[11] J. Jamisola, S. Rodrigo, A. M. Anthony and G. R. Rodney, "Failure-tolerant path planning for kinematically redundant manipulators anticipating locked-joint failures," *Robotics, IEEE Transactions* on 22.4, 603-612, 2006.

[12] R. Boudreau, and N. Scott, "Force Optimization of kinematically-redundant planar parallel manipulators following a desired trajectory," *Mechanism and Machine Theory*, 56, 138-155, 2012.

[13] Y. Oh, W. Chung and Y. Youm, "Extended impedance control of redundant manipulators based on weighted decomposition of joint space. *Journal of Robotic Systems*, Vol. 15(5), pp. 231-258, 1998.

[14] M. Z. Ding, C. J. Ong, and A.N. Poo, "Resolution of redundant manipulator via distance optimization," *Proc. of the Inst. of Mech. Eng, Journal of Mechanical Engineer Scince*, Vol. 204, No: 8, 2000

[15] A. R. Cherif, V. Perdereau and M. Droin, M., "Penalty approach for a constrained optimization to solve on-line to the inverse kinematic problem of redundant manipulators," *Proceedings of the 1996 IEEE International Conference on Robotics and Automation*, Minneapolis-Minnesota, April 1996

[16] A. Khoukhi, L. Baron, M. Balazinski and K. Demirli, "Hybrid neuro-fuzzy multi-objective trajectory planning of redundant manipulators. *Journal of Control and Intelligent Systems*, Vol.37, No:2, 2009.

[17] X. Luo and W. Wei, "A new immune genetic algorithm and its application in redundant manipulator path planning," *Journal of Robotic Systems,* Vol. 21(3), pp. 141-151, 2004.

[18] A. Müller, and T. Hufnagel, "Model-based control of redundantly actuated parallel manipulators in redundant coordinates," *Robotics and Autonomous Systems*, 60(4), 563-571, 2012.

[19] W. Shang and C. Shuang, "Nonlinear computed torque control for a high-speed planar parallel manipulator," *Mechatronics*, 19.6: 987-992, 2009.

[20] A. Jahed, F. Piltan, H. Rezaie and B. Boroomand, "Design computed torque controller with parallel fuzzy inference system compensator to control of robot manipulator," *International Journal of Information Engineering & Electronic Business*, 5(3), 2013.

[21] A. Elkady, G. Elkobrosy, S. Hanna and T. Sobh, "Cartesian parallel manipulator modeling, control and simulation," *INTECH Open Access Publisher*, 2008.

[22] N. Kumar, V. Panwar, N. Sukavanam, S .P. Sharma and J. H. Borm, "Neural network-based nonlinear tracking control of kinematically redundant robot manipulators," *Mathematical and Computer Modeling*, 53(9), 1889-1901, 2011.

[23] B. Daachi, T. Madani and A. Benallegue, "Adaptive neural controller for redundant robot manipulators and collision avoidance with mobile obstacles," Neurocomputing 79: 50-60, 2012.

[24] A. Ayman, O. Hidetoshi and A. A. Ahmed, "Adaptive control of a parallel robot using fuzzy inverse model," *International Journal Of Control, Automation and Systems* Vol. 1, No. 1, January 2012.

[25] L. Tian and C. Collins, "An effective robot trajectory planning method using a genetic algorithm," *Mechatronics* 14.5: 455-470, 2004.

[26] A. Bayram, and M. K. Özgören, "the conceptual design of a spatial binary hyper redundant manipulator and its forward kinematics," *Proc IMechE, Part C: J. Mechanical Engineering Science*, vol. 226, no. 1, p. 217–227, 2012.

[27] M. K. Özgören, "Kinematic analysis of spatial mechanical systems using exponential rotation matrices," *Journal of Mechanical Design, ASME*, Vol. 129, pp. 1144-1152, 2007

[28] B. Dasgupta, and T. S. Mruthyunjaya, "A Newton-Euler formulation for the inverse dynamics of the Stewart platform manipulator," Mechanism and Machine Theory, 1998, 33.8: 1135-1152.7, 1998

[29] H. Abdellatif and B. Heımann, "Computational efficient inverse dynamics of 6-DOF fully parallel manipulators by using the Lagrangian formalism," *Mechanism and Machine Theory*, 2009, 44.1: 192-207, 2009

[30] McPhee, J., P. Shi. and Piedbuf, J-C., (2002), Dynamics of multibody systems using virtual work and symbolic programming. Mathematical and Computer Modelling of Dynamical Systems 8.2 (2002): 137-155.

[31] M. Mitchell, "An introduction to genetic algorithms," 5th Ed., *The MIT Press,* 1999

Atilla Bayram was born in Van-Turkey in 1973. He received the B.S. degree in mechanical engineering from Gazi University, Ankara, Turkey, in 1995 and the M.S. and Ph.D. in mechanical engineering, from Yuzuncu Yil University, Van, Turkey in 2001 and The Middle East Technical University, Ankara, Turkey, in 2010, respectively. He worked as a research assistant in Yuzuncu Yil University and The Middle East Technical University during 1998-2010. After that time, he has been working as an Assistant Professor in Yuzuncu Yil University. His current research interests are in robot control, system identification and dynamics.